Ninth International Conference on CFD in the Minerals and Process Industries
CSIRO, Melbourne, Australia
10-12 December 2012

HIGHLY RESOLVED SIMULATIONS OF SOLIDS SUSPENSION IN A MIXING TANK

Jos DERKSEN

Chemical & Materials Engineering, University of Alberta, Edmonton, Alberta, CANADA
jos@ualberta.ca

ABSTRACT

Direct simulations of a solids suspension process in a mixing tank have been performed. The simulations fully resolve the mildly turbulent liquid flow (Re≈2,000), and the motion of a few thousand spherical particles. Solids and liquid dynamics are tightly coupled by imposing no-slip at the solids surfaces through an immersed boundary method and using the resolved hydrodynamic forces to update the motion of the solid particles. The flow is solved by means of a lattice-Boltzmann method. In addition to being moved by hydrodynamic forces, the particles feel gravity, and undergo hard-sphere collisions, the latter according to an event-driven algorithm. Solids volume fractions are of order 0.1. The simulations show the start-up of the solids suspension process from an initial state with zero velocity and all particles forming a granular bed on the bottom of the tank. Steady state distributions of solids in the tank are established through the interplay of net gravity, hydrodynamic forces, and collisions between particles.

NOMENCLATURE

Ar	Archimedes number
a	sphere radius
D	impeller diameter
e	restitution coefficient
$\mathbf{g}$	gravitational acceleration vector
H,L	tank dimensions
M	total number of spheres
N	impeller rotation rate
Re	Reynolds number
$\mathbf{r}$	location vector
s	geometric constant in Zwietering correlation
t	time
U_∞	(single sphere) settling velocity
$\mathbf{u}$	fluid velocity vector
$\mathbf{u_p}$	particle velocity vector
v_{tip}	impeller tip speed
z,z_p	vertical (particle) coordinate
Δ	lattice spacing
η	Kolmogorov length scale
μ	friction coefficient
θ	Shields number
ν	kinematic viscosity
ρ,ρ_s	liquid density, solids density
ϕ	solids volume fraction
Ω	impeller angular velocity

INTRODUCTION

Solid particles suspended in liquid flows are very common: rivers carrying sediment, slurries being transported through pipelines, powders being dissolved in water, crystalline material being formed and growing in agitated crystallization reactors are just a few examples. The dynamical behavior of solid-liquid suspensions is the result of an intricate interplay between the dynamics of the liquid phase and the solids phase, and the research on this topic has a long and rich tradition (Stokes, 1901; Richardson & Zaki, 1954; Batchelor, 1971; Guazzelli, 2001; Guazzelli & Hinch, 2011) For a large part this research effort is driven by practical relevance: the design of pipelines for transporting slurries, or the assessment of reactor performance that depends on solid-liquid mass transfer (dissolution, crystal growth, solids carrying catalytic material for liquid-phase reactions) requires knowledge of how the solids distribute themselves in the liquid phase as a result of hydrodynamic forces, net gravity (or buoyancy), and collisions between the solids, or between solids and bounding walls.

The more interesting situations are those with moderate to high solids volume fractions, solid over fluid density ratios of order one, and solid particle sizes that overlap with fluid dynamics length scales, e.g. a turbulent flow with particles larger than the Kolmogorov scale. In such situations the solid particles feel a complex hydrodynamic environment. Where fluid-solid interactions in gas-solid systems (high density ratios) are dominated by the drag force, liquid-solid systems are governed by a broader gamut of forces (Maxey & Riley, 1983). Furthermore, in dense (i.e. high solids-volume-fraction) suspensions, particles interact strongly with one another, through the liquid and as a result of direct interaction (collisions). This complexity makes it challenging to predict the behavior of dense, agitated solid-liquid suspensions.

There is no universal approach for modeling and simulation of suspension flows. The appropriate methods depend on the flow regime (as estimated based on Stokes numbers, Reynolds numbers, solids volume fractions, density ratios, and possibly particle shapes), and on the levels of detail and accuracy required. It is important to note, however, that none of the approaches is fully predictive. At various levels, assumptions, sub-models, or empirical correlations are needed to account for unresolved parts of the suspension physics (one can think of hydrodynamic force correlations, assumptions regarding the dynamic coupling of fluid and solid, parameterizations related to continuum descriptions of the solids phase as in kinetic theory of granular matter, e.g.

Gidaspow, 1994). Usually the finer (length) scales are parameterized, and the larger scales are resolved. There is, however, a need for simulations that resolve down to finer scales and require little parameterization. We can think of three main reasons: (1) The relevance of what happens at short length scales for process performance (mass transfer, mechanical load on solids, liquid deformations); (2) The assessment of existing sub-models and assumptions for parameterizing small scales; (3) The development of new parameterizations.

There obviously is a computational penalty for resolving down to finer scales: the physical size of the domains that can be simulated gets limited. In very impressive simulations by Lucci et al (2010) on resolved solid particles in homogeneous, isotropic turbulence, the domain size was typically 32 times the particle size. With sand-grain size particles (order 0.3 mm) this implies a domain with linear size of 1 cm which is much smaller than typical process equipment operated under turbulent conditions. Limitations on domain size are a reason for using fully periodic boundary conditions in such highly resolved simulations. The simulated domain is a small sample (a meso-scale sample) of what is happening in a large, essentially unbounded domain, away from walls. This is an Achilles heel of such fully periodic mesoscopic simulations: they are not able to directly account for geometric effects (walls, impellers, internal hardware), and (related to this) it is hard to mimic fully periodic conditions in an experiment. Physical experiments are in great need; highly resolved ('direct') simulations of solid-liquid suspension flow still need validation. Complete resolution of all relevant dynamic scales is not possible. Resolving the flow around individual particles is very well possible; resolving e.g. their surface roughness (a typically 100 times finer length scale compared to the particle size) is not. Surface roughness is usually parameterized by a friction coefficient that allows for tangential momentum exchange when two particles collide. Similar resolution issues play a role when particles are in very close proximity. On fixed computational grids the hydrodynamic interactions get under-resolved; adaptive grids are not truly an option for simulating the interactions between a significant number (>10) of particles. On fixed grids, models for lubrication forces are then applied to mitigate these resolution issues.

With the above in mind, highly resolved simulations of dense solid-liquid suspensions in mildly turbulent flow were performed. The geometry (a miniature mixing tank with a linear size of a few centimeters, and mm size spherical particles) was designed such that it on one side allows for simulations with resolved particles, and on the other side for reproducing it in a laboratory. The goal of this work is to invite experimentalists to mimic the flow systems presented here, and to (as detailed as possible) visualize the suspension (liquid and solid) dynamics. Such an interaction between experiment and simulation would greatly help in making thoughtful choices regarding parameterizations and numerics (grid resolution, time step, numerical method), and (hopefully) in building confidence in highly resolved simulations.

The work presented here is based on our earlier work on resolved simulations of solid-liquid suspensions (mainly in periodic domains) (Ten Cate et al, 2004; Derksen & Sundaresan, 2007), and on detailed simulations of mixing (Derksen & Van den Akker, 1999). Many numerical and verification issues have been discussed in these earlier papers. For turbulent mixing flows these include validation by means laser Doppler anemometry data and assessment of grid effects. For relatively simple solid-liquid systems we performed experimental validation for a single settling sphere (Ten Cate et al, 2002), and compared simulation results with analytical solutions under creeping flow conditions (Derksen, 2008). The insights regarding these earlier works have been used in this paper. As a result we will only briefly explain the numerical method, and will not perform a grid sensitivity study for the specific flow systems at hand. The focus of the paper will be on describing the flow field results, and on understanding how they depend on operating conditions in an experimentally verifiable manner.

The organization of this paper is as follows: In the next section the flow system is defined in terms of its geometry and dimensionless numbers. Subsequently the numerical procedure is outlined. It is based on a lattice-Boltzmann (LB) method for resolving the liquid flow, an immersed boundary method for representing no slip conditions at solid surfaces (particle surfaces and the impeller), and hard-sphere collisions between particles. In the *Results* section first qualitative impressions of the suspension flow are given and its development towards a dynamically steady state is described. In analyzing the results we focus on the distribution of solids through the tank. The final section summarizes the main findings.

FLOW SYSTEM

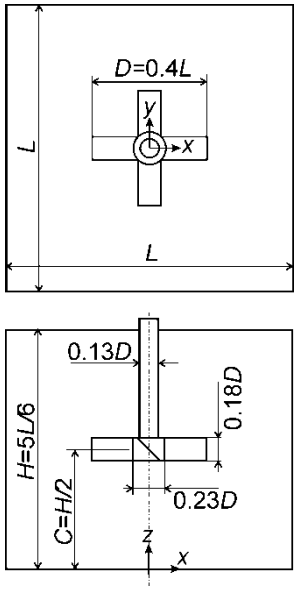

Figure 1: Flow geometry and Cartesian coordinate system. Top: top view; bottom: side view. The tank is closed off with a lid that acts as a no-slip wall. In addition to the dimensions given in the figure, the thickness of the impeller blades is $0.021D$. The impeller rotates such that it pumps liquid downward.

The layout of the flow geometry along with a definition of the coordinate system is given in Figure 1. Gravity points in the negative z-direction: $\mathbf{g} = -g\mathbf{e}_z$. The tank has a square cross section with side-length L. The height of the tank is $H = 5L/6$. An impeller is placed in the center of the tank's cross section and with the middle of the impeller halfway the height of the tank (i.e. at $z = H/2$).

It is a pitched-blade turbine: four flat blades are mounted under 45° on a cylindrical hub that is attached to the shaft. The impeller diameter is $D = 2L/5$. The shaft enters the tank from the top. The impeller rotates with an angular velocity of $\Omega = 2\pi N$ (rad/s) with rotational direction such that it pumps downward. The tank is filled up to a level $z=H$ and closed off with a lid so that no-slip conditions apply all around.

The tank contains a Newtonian liquid with density ρ and kinematic viscosity ν and we define the impeller Reynolds number as $\mathrm{Re} = ND^2/\nu$. The tank also contains spherical solid particles. They are uniformly sized with radius *a*. The solid over liquid density ratio has been fixed to $\rho_s/\rho = 2.5$ (typical for e.g. glass beads in a watery liquid). The solids volume fraction has been set for all cases to $\phi = \dfrac{V_s}{L^2H - V_i} = 0.083$ with V_s to the total solids volume (i.e. $V_s = M\,4\pi a^3/3$ for M spheres), and $V_i = 0.0018L^3$ the volume of the impeller plus shaft.

Gravitational acceleration has been non-dimensionalized through the introduction of $\theta = \dfrac{\rho N^2 D^2}{g(\rho_s - \rho)2a}$. The group θ we view as a variant of the Shields number $\theta = \dfrac{\sigma}{g(\rho_s - \rho)2a}$ that is widely used for characterizing erosion of granular beds by fluid flow (Ouriemi et al 2007). Traditionally the stress σ is a viscous shear stress (then $\sigma = \rho\nu\dot{\gamma}$ with $\dot{\gamma}$ the shear rate). The Shields number reflects the competition between gravity pulling solids to the bottom of the tank, and hydrodynamic stress suspending the particles. Since the flow in the tank is dominated by inertia, we have introduced a measure for the inertial stress $\rho N^2 D^2$ rather than a viscous stress in the Shields number.

It is instructive to interpret the above definition of the Shields number in terms of the classical results due to Zwietering (1958) on solids suspension in mixing tanks. He performed an extensive set of solids suspension experiments with particles having a narrow size distribution and summarized the results in a correlation that carries his name. In terms of the symbols as defined above the Zwietering correlation reads

$$N_{js} = \frac{s(2a)^{0.2}\nu^{0.1}(100\phi\rho_s/\rho)^{0.13}}{D^{0.85}}\left(\frac{g(\rho_s - \rho)}{\rho}\right)^{0.45} \quad (1)$$

with N_{js} the just-suspended impeller speed, i.e. the minimum rate of agitation to keep all solids suspended (more precisely defined in Zwietering, 1958); and *s* a geometry dependent parameter (in the range 2 to 20). The term $100\phi\rho_s/\rho \equiv \Phi_m$ represents the solids mass fraction as a percentage. If a critical (or just-suspended) Shields number is defined as $\theta_{js} = \dfrac{\rho N_{js}^2 D^2}{g(\rho_s - \rho)2a}$, the Zwietering correlation (Eq. 1) can be written as

$$\theta_{js} = s^2\Phi_m^{0.26}\mathrm{Ar}^{-0.1}\left(\frac{2a}{D}\right)^{-0.3} \quad (2)$$

It implies that the critical Shields number depends on the solids mass fraction, a particle size over impeller diameter aspect ratio and (only weakly; power −0.1) on the Archimedes number $\mathrm{Ar} \equiv \dfrac{g(\rho_s - \rho)}{\rho\nu^2}(2a)^3$. The specific situations that were simulated were chosen based on possibilities for experimental verification (this e.g. led to the density ratio of 2.5), our desire to have a fairly dense suspension under (mildly) turbulent conditions, and computational feasibility. Computational feasibility limits the number of particles to a few thousand, and it limits the impeller Reynolds number since all turbulent scales need to be resolved.

We define our base-case in terms of dimensionless numbers in Table 1. As an example of a physical system that has these characteristics, the particles can be assumed to be spherical glass beads with a diameter of 1.0 mm. The impeller then has a diameter of *D*=1.2 cm, and the sides of the tank are *L*=3.0 cm. Since *g*=9.8 m/s^2, and θ=24.0, the impeller speed is *N*=49.5 rev/s. In order to achieve Re=1,920, the kinematic viscosity of the liquid needs to be $\nu = 3.71\cdot10^{-6}$ Pa·s (which can be achieved by e.g. making a glycerol-water mixture).

Re	1920
M	3600
ϕ	0.083
ρ_s/ρ	2.5
D/a	24.0
θ	24.0
H/L	5/6
D/L	0.40

Table 1: Definition of the base-case in terms of dimensionless numbers.

If we take *s*=6 as an order-of-magnitude estimate for the geometrical parameter in Eq. 1 (see e.g. the propeller data in Zwietering, 1958) then N_{js}=92 rev/s (and θ_{js}=83) for the physical system defined above. This is almost twice as high as the base-case impeller speed. As a consequence we do not expect fully suspended solids for the base-case. The variations from the base case to be discussed later are with respect to the Shields number that has been varied in the range $6 \le \theta \le 96$.

The flow systems are started by creating a random packing of particles on the bottom of the tank. This granular bed has a thickness of approximately $8a$, i.e. equivalent to four layers of spheres. The impeller is situated well above this bed. Then the impeller is set to rotate, which agitates the liquid and subsequently causes erosion of the granular bed and solids getting suspended in the liquid. This procedure allows us to study the start-up of the suspension process. It is a scenario that can be mimicked experimentally, albeit with some care related to the speed of image acquisition. As we will see, the start-up phase of the solids suspension process takes a few tens of impeller revolutions which (in the physical system) is of the order of one second.

MODELING APPROACH

We used the lattice-Boltzmann (LB) method (Chen & Doolen, 1998; Succi, 2001) to solve for the liquid flow. The specific scheme employed here is due to Somers (1993). The method has a uniform, cubic grid (grid spacing Δ). The resolution was such that the side length L was represented by 360 grid spacings ($L = 360\Delta$). A crude estimate of the smallest turbulent length scale (crude because it is based on fully developed turbulence which is clearly not the case here) in the tank is $\eta = D\mathrm{Re}^{-3/4} \approx 0.5\Delta$. Our resolution therefore satisfies the typical criterion for sufficiently resolved direct numerical simulations of turbulence: $\Delta < \pi\eta$ (Eswaran & Pope, 1998).

The no-slip boundary conditions at the outer walls of the tank were implemented according to the half-way bounce-back rule (Succi, 2001). The no-slip conditions at the particles' surfaces and at the impeller surface were dealt with by means of an immersed boundary (or forcing) method (Derksen & Van den Akker, 1999; Ten Cate et al, 2002). In this method, the surfaces are defined as sets of closely spaced points (the typical spacing between points is 0.7Δ), not coinciding with lattice points. At these points the (interpolated) fluid velocity is forced to the local velocity of the solid surface according to a control algorithm. The impeller undergoes a predefined rotational motion so that we know the location and velocity of each of its surface points at any moment in time. The local particle surface velocity has contributions from translational and rotational motion of the sphere under consideration. Adding up (discrete integration) per spherical particle of the forces needed to maintain no-slip provides us with the (opposite; action equals minus reaction) force the fluid exerts on the spherical particle. Similarly the hydrodynamic torque exerted on the particles can be determined. Forces and torques are subsequently used to update the linear and rotational equations of motion of each spherical particle. This update determines the new locations and velocity of the sphere surface points that are subsequently used to update the liquid flow, and so forth.

It should be noted that having a spherical particle on a cubic grid requires a calibration step, as earlier realized by Ladd (1994). He introduced the concept of a hydrodynamic radius. The calibration involves placing a sphere with a given radius a_g in a fully periodic cubic domain in creeping flow and (computationally) measuring its drag force. The hydrodynamic radius a of that sphere is the radius for which the measured drag force corresponds to the expression for the drag force on a simple cubic array of spheres due to Sangani & Acrivos (1982). Usually a is slightly larger than a_g with $a - a_g$ typically equal to half a lattice spacing or less. The simulations presented in this paper have a resolution such that $a = 6\Delta$.

Experimental validation and grid refinement studies show that a resolution of 6 lattice-spacings over a sphere radius is sufficient for resolving the flow around a solid sphere for particle Reynolds numbers based on slip velocity up to order 50 (Ten Cate et al, 2002). The particle Reynolds number based on its settling velocity U_∞ for the base-case is $\mathrm{Re}_{p\infty} = U_\infty 2a/\nu \approx 25$, i.e. less than 50. To obtain this estimate the Schiller & Naumann (1933) drag correlation was used: $C_D = \frac{24}{\mathrm{Re}}\left(1 + 0.15\,\mathrm{Re}^{0.687}\right)$. An upper bound of the particle Reynolds number in our simulations would be based on a particle slip velocity equal to the impeller tip speed: $\mathrm{Re}_{p,tip} = \pi ND 2a/\nu$ =400 which is markedly higher than 50. The impeller tip speed, however, is a measure for the maximum liquid velocity in the tank, and slip velocities (the local difference of liquid and solid velocity) will generally be much smaller than the tip speed. Still, spatial resolution of the flow around the spheres is a concern and will be assessed by determining the way $\mathrm{Re}_p = u_{slip} 2a/\nu$ is distributed in the tank for the base-case simulation.

The temporal resolution was such that one revolution of the impeller took 3600 time steps: $N = \frac{1}{3600\Delta t}$. The convective time scales of the particles $\frac{a}{U_\infty}$ and $\frac{a}{\pi ND}$ were $960\,\Delta t$ and $48\,\Delta t$ respectively so that a particle only moves a (very) small fraction of its radius over one time step.

The spheres directly interact through hard-sphere collisions according to the two-parameter model (restitution coefficient e and friction coefficient μ) due to Yamamoto et al (2001). The same e and μ were also used when a sphere hits one of the bounding walls. Different from gas-solid systems, in liquid-solid systems the choice of the restitution coefficient is not critical for the overall suspension behavior. This is because energy dissipation largely takes place in the liquid phase, not so much during dry collisions. The restitution coefficient was set to e=1 throughout this work. Recent results on erosion of granular beds by laminar flow suggest a more critical role for the friction coefficient (Derksen, 2011). Friction allows particles to exchange angular momentum (or to transfer linear momentum to angular momentum and vice versa), and therefore allows rolling of particles (over one another or over walls) which is very relevant for solids in a dense granular bed or resting on a wall being mobilized by fluid flow. Our results on erosion (Derksen, 2011) show that a zero or a non-zero μ makes a significant difference, with the precise value of a non-zero μ being less relevant (results with μ=0.1 and μ=0.25 showed minor differences). Since with μ=0.1 we were able to well reproduce experimental data on critical Shields numbers, that value for μ was used in the current work as well.

Collisions between solid spheres and the impeller are modeled according to a scenario akin to soft-sphere collisions: each time step it is checked if sphere volume and impeller volume overlap. If so, we determine the component of the relative velocity of the impeller and the particle in the direction normal to the impeller surface: $u_r = \left[\mathbf{u_p} - \left(\mathbf{\Omega}\times\mathbf{r}\right)\right]\cdot\mathbf{n}$ with $\mathbf{r}$ the location of particle-impeller contact, and $\mathbf{n}$ the unit normal to the impeller surface. Subsequently the relative velocity is reverted: $\tilde{\mathbf{u}}_\mathbf{p} = \mathbf{u_p} - 2u_r\mathbf{n}$ with $\tilde{\mathbf{u}}_\mathbf{p}$ the post-collision particle velocity. This procedure limits overlap of any sphere with the impeller to 0.5% of the sphere volume at maximum, and the interaction time between sphere and impeller to 5 time steps (corresponding to 0.5° of impeller rotation).

The fixed-grid simulations involving moderately dense suspensions as discussed here require explicit inclusion of

sub-grid lubrication forces. Here we follow the procedure proposed by Nguyen & Ladd (2002) that we have previously used for e.g. liquid-fluidized bed simulations (Derksen & Sundaresan, 2007).

The spheres' equations of linear and rotational motion including resolved and unresolved (i.e. lubrication) forces are integrated according to an explicit split-derivative method (Feng & Michaelides, 2009). These time-step driven updates are linked with an event-driven algorithm that detects and carries out hard-sphere collisions and sphere-outer-wall collisions during the time steps. Once an event is being detected, all particles are frozen and the event is carried out which implies an update of the linear velocities (and also angular velocities if $\mu \neq 0$) of the sphere(s) involved in the event. Subsequently all spheres continue moving until the end of the time step, or until the next event, whatever comes first. The hard-sphere algorithm has been verified by carrying out granular simulations (no interstitial fluid). Zero-overlap of sphere volumes, and exact energy conservation (if e=1 and μ=0) have been confirmed.

RESULTS

Impressions of the Base-Case Simulation

The way the solids gets suspended upon starting the impeller at t=0 is depicted in Figure 2. The figure also shows contours of the liquid velocity magnitude in the mid plane. The downward impeller stream is clearly visible. It extends to the granular bed where it is responsible for mobilizing the solid particles in the upper layer of the bed. The erratic structure of the impeller stream shows the transitional / turbulent (or at least the non-laminar)

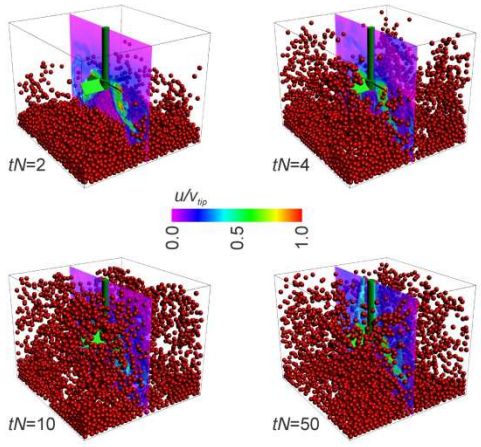

Figure 2: Evolution of the solids suspension process: instantaneous realizations of particle locations and liquid flow (in the mid-plane) at four moments as indicated. Base-case conditions.

nature of the liquid flow. After 10 impeller revolutions many particles have been mobilized. The particles in the bottom corners, however, have hardly moved at this stage. The base-case simulation was stopped after 50 impeller revolutions when a dynamic steady state was reached as can be witnessed from Figure 3. It shows the average vertical location of the particles, and the standard deviation. At the start of the process the average as well as the standard deviation increases quickly. The average vertical particle location reaches an absolute maximum of approximately $\langle z_p \rangle \approx 0.36H$ after 10 impeller revolutions. It then decreases to a (dynamically) steady state value of around $0.3H$ after some 20 impeller revolutions. The overshoot is a clear manifestation of two-way coupling between liquid flow and solid particle motion: the liquid flow weakens as a result of the presence of suspended particles because next to liquid, the impeller has to pump around (relatively heavy and inert) particles. The weakening of the liquid flow is not instantaneous due to finite inertia of liquid and solids; it takes time for the suspension flow to adapt itself to changing conditions. Some of the trends in the average vertical particle location can be linked to specific events. For instance, the relatively quick decline around tN=20 is due to the collapse of stacks of particles in the bottom corners of the tank. The time scales of the slow fluctuations in the standard deviation of vertical particle position (Figure 3) are comparable to those of the average position. The standard deviation does not show an overshoot.

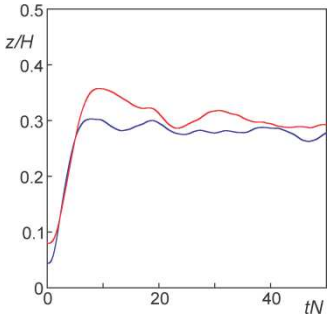

Figure 3: Time series of the average vertical location of the particles $\langle z_p \rangle \equiv \frac{1}{M}\sum_{i=1}^{M} z_{pi}$ (red line) and the rms value of the vertical particle location $z_p' \equiv \sqrt{\frac{1}{M}\sum_{i=1}^{M}\left[z_{pi} - \langle z_p \rangle \right]^2}$ (blue line). Base-case conditions.

Above we expressed concerns regarding the resolution of the flow around the spheres. To check this further, the distribution of particle Reynolds numbers based on the slip velocity is given in Figure 4. There we show four distributions that are very similar. They relate to two independent instant realizations of the flow and two ways for estimating the liquid velocity in the spheres' vicinity. To determine the slip velocity, the liquid velocity in the vicinity of each sphere was spatially averaged in a cube-sized volume with side lengths $3a$ and $4a$. It can be concluded that at any moment some 20% of the spheres has $\mathrm{Re}_p > 50$ which indicates some lack of spatial resolution.

The base-case results as presented so far indicate that a dynamically steady state is reached 20 impeller revolutions after start-up. This allows us to present time-averaged results with an averaging window from tN=20 to tN=50. The time-averaged distribution of solids is given in Figure 5. The vertical cross section shows preferential locations underneath the impeller and closely above the

bottom of the tank. The horizontal cross section closely above the bottom (at $z=a$) reveals the action of the impeller stream sweeping particles over and away from the bottom. Particles are (on average) removed from the bottom in the middle of the edges where the impeller stream is felt strongest; they collect in the corners and in the center of the tank bottom.

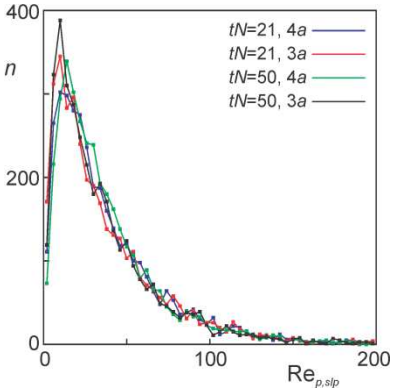

Figure 4: Distribution of particle Reynolds numbers based on the particle-liquid slip velocity $\mathrm{Re}_{p,slp} = \left|\mathbf{u_p} - \mathbf{u}\right| 2a / \nu$ at two instantaneous realizations of the flow (21 and 50 impeller revolutions after start-up). The liquid velocity **u** was the average velocity in the surroundings of the solid particle. As the surroundings, cubes with sides 3a and 4a around the particles were considered. Base-case conditions.

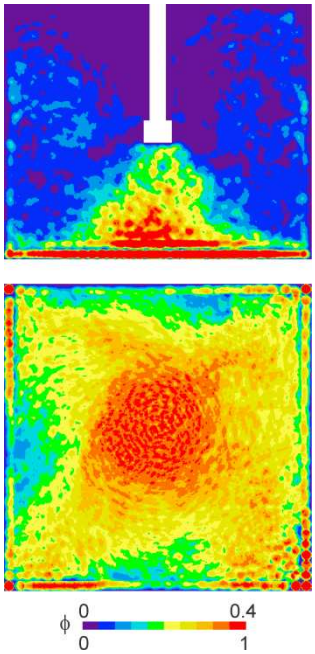

Figure 5: Time-average solids volume fraction in the vertical mid-plane (top), and in the horizontal plane with $z=a$ (bottom). The time window for averaging is tN=20 – 50. Base-case conditions. The two panels have different color scales: the upper scale for the upper panel; the bottom scale for the bottom panel. In the view of the bottom panel, the impeller rotates in the clockwise direction.

Shields Number Effects

As a final *Results* sub-section we briefly present impressions as to how the solids suspension process depends on the Shields number. Figure 6 shows instantaneous realizations for four Shields numbers at instances after steady state was reached. Clearly the levels to which particles rise depends on θ. The latter is further quantified in Figure 7 that shows time series of the average vertical particle location from start-up as granular beds to dynamically steady states. The average vertical location $\langle z_p \rangle \approx 0.5H$ for θ=96 which indicates complete suspension.

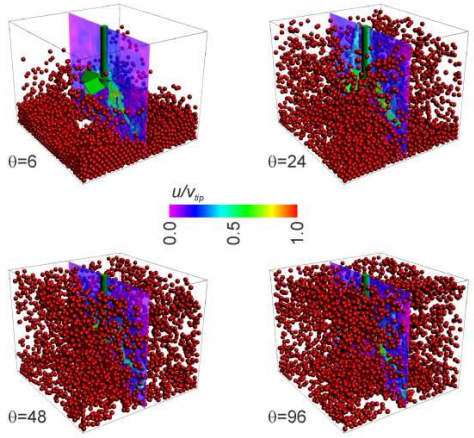

Figure 6: Instantaneous realizations after steady state has been reached for different Shields numbers θ as indicated.

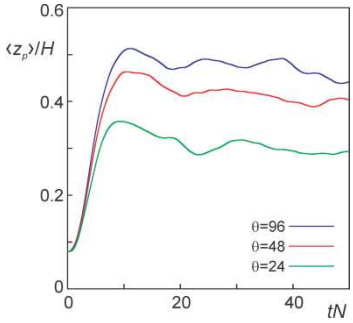

Figure 7: Time series of the average vertical location of the particles for three values of θ as indicated.

SUMMARY

In this paper results of highly resolved simulations of solids suspension processes in mixing tanks were presented. They need minimal modeling input: the mildly turbulent flow was fully resolved and so were the hydrodynamic forces on the particles. Only when particles get very close to one another, modeling enters the simulation procedure: Lubrication forces were added to represent close range hydrodynamic interactions, and collision parameters (specifically the friction coefficient) were used to model solid surface properties (specifically its roughness).

The results show a realistic start-up of the suspension process and a clear dependency on the Shields number.

The simulations are designed such as to make experimental validation feasible, and clearly this should be the next step in this research.

REFERENCES

BATCHELOR, G.K., (1972), "Sedimentation in a dilute dispersion of spheres", *J. Fluid Mech*., **52**, 245-268.

CHEN, S. and DOOLEN, G.D., (1998), "Lattice-Boltzmann method for fluid flows", *Annu. Rev. Fluid Mech*. 30, 329-364.

DERKSEN, J. and VAN DEN AKKER, H.E.A., (1999), Large-eddy simulations on the flow driven by a Rushton turbine. *AIChE J*., 45: 209-221.

DERKSEN, J.J. and SUNDARESAN, S., (2007), "Direct numerical simulations of dense suspensions: wave instabilities in liquid-fluidized beds", *J. Fluid Mech*., **587**, 303-336.

DERKSEN, J.J., (2008), "Flow-induced forces in sphere doublets", *J. Fluid Mech*., **608**, 337-356.

DERKSEN, J.J., (2011), "Simulations of granular bed erosion due to laminar shear flow near the critical Shields number", *Phys. Fluids*, **23**, 113303.

ESWARAN, V. and POPE, S.B., (1998) "An examination of forcing in direct numerical simulations of turbulence", *Comput. Fluids*, **16**, 257–278.

FENG, Z.G. and MICHAELIDES, E., (2009), "Robust treatment of no-slip boundary condition and velocity updating for the lattice-Boltzmann simulation of particulate flows", *Comput. Fluids*, **38**, 370-381.

GIDASPOW, G., (1994), *Multiphase flow and fluidization: Continuum and kinetic theory descriptions*. Academic Press, San Diego.

GUAZZELLI, É., (2001), "Evolution of particle-velocity correlations in sedimentation", *Phys. Fluids*, **13**, 1537-1540.

GUAZZELLI, É. and HINCH, J., (2011), "Fluctuations and instability in sedimentation", *Annu. Rev. Fluid Mech*., **43**, 97-116.

LADD, A.J.C., (1994) "Numerical simulations of particle suspensions via a discretized Boltzmann equation. Part I: Theoretical Foundation", *J. Fluid Mech*., **271**, 285-309.

LUCCI, F., FERRANTE, A. and ELGHOBASHI, S., (2010), "Modulation of isotropic turbulence by particles of Taylor length-scale size", *J. Fluid Mech*., **650**, 5–55.

MAXEY, M.R. and RILEY, J.J., (1983), "Equation of motion for a small rigid sphere in a nonuniform flow", *Phys. Fluids*, **26**, 883-889.

NGUYEN, N.-Q. and LADD, A.J.C., (2002), "Lubrication corrections for lattice-Boltzmann simulations of particle suspensions", *Phys. Rev*. E, **66**, 046708.

OURIEMI, M., AUSSILLOUS, P., MEDALE, M., PEYSSON, Y. and GUAZZELLI, E., (2007), "Determination of the critical Shields number for particle erosion in laminar flow", *Phys. Fluids*, **19**, 061706.

RICHARDSON, J.F. and ZAKI, W.N., (1954), "The sedimentation of a suspension of uniform spheres under conditions of viscous flow", *Chem. Engng. Sc*., **8**, 65-73.

SANGANI, A.S. and ACRIVOS, A., (1982) "Slow flow through a periodic array of spheres", *Int. J. Multiphase Flow*, **8**, 343-360.

SCHILLER, L. and NAUMANN, A., (1933) "Uber die grundlagenden Berechnungen bei der Schwerkraftaufbereitung", *Ver. Deut. Ing. Z*., **77**, 318–320.

SOMERS, J.A., (1993), "Direct simulation of fluid flow with cellular automata and the lattice-Boltzmann equation", *App. Sci. Res*., **51**, 127-133.

STOKES, G.G., (1901), *Mathematical and Physical Papers, Volumes I-V*. Cambridge University Press.

SUCCI, S., (2001), *The lattice Boltzmann equation for fluid dynamics and beyond*. Clarendon Press, Oxford.

TEN CATE, A., NIEUWSTAD, C.H., DERKSEN, J.J. and VAN DEN AKKER, H.E.A., (2002), "PIV experiments and lattice-Boltzmann simulations on a single sphere settling under gravity", *Phys. Fluids*, **14**, 4012-4025.

TEN CATE, A., DERKSEN, J.J., PORTELA, L.M. and VAN DEN AKKER, H.E.A., (2004), "Fully resolved simulations of colliding spheres in forced isotropic turbulence", *J. Fluid Mech*., **519**, 233-271.

YAMAMOTO, Y., POTTHOFF, M., TANAKA, T., KAJISHIMA, T. and TSUJI, Y., (2001), "Large-eddy simulation of turbulent gas-particle flow in a vertical channel: effect of considering inter-particle collisions", *J. Fluid Mech*., **442**, 303-334.

ZWIETERING, Th.N., (1958), "Suspending of solid particles in liquid by agitators", *Chem. Engng. Sc*., **8**, 244-253.

